Bioactive Materials 15 (2022) 103–119

Contents lists available at ScienceDirect

Bioactive Materials

journal homepage: www.keaipublishing.com/en/journals/bioactive-materials

A conductive supramolecular hydrogel creates ideal endogenous niches to promote spinal cord injury repair

Biao Yang [a,b,c,1], Chengzhen Liang [a,b,c,1], Di Chen [d,1], Feng Cheng [a,b,c], Yuang Zhang [a,b,c], Shaoke Wang [a,b,c], Jiawei Shu [a,b,c], Xianpeng Huang [a,b,c], Jingkai Wang [a,b,c], Kaishun Xia [a,b,c], Liwei Ying [a,b,c], Kesi Shi [a,b,c], Chenggui Wang [a,b,c], Xuhua Wang [a,f], Fangcai Li [a,b,c,***], Qian Zhao [e,**], Qixin Chen [a,b,c,*]

[a] Department of Orthopedics Surgery, The Second Affiliated Hospital, School of Medicine, Zhejiang University, Hangzhou, 310009, Zhejiang, China
[b] Orthopedics Research Institute of Zhejiang University, Hangzhou, 310009, Zhejiang, China
[c] Key Laboratory of Motor System Disease Research and Precision Therapy of Zhejiang Province, Hangzhou, 310009, Zhejiang, China
[d] Ningbo Research Institute of Zhejiang University, Ningbo, 315100, Zhejiang, China
[e] State Key Laboratory of Chemical Engineering, College of Chemical and Biological Engineering, Zhejiang University, Hangzhou, 310027, Zhejiang, China
[f] NHC and CAMS Key Laboratory of Medical Neurobiology, MOE Frontier Science Center for Brain Research and Brain-Machine Integration, School of Brain Science and Brain Medicine, Zhejiang University, Hangzhou, 310003, Zhejiang, China

ARTICLE INFO

Keywords:
Conducting polymer
Supramolecular hydrogels
Biomimetic scaffolds
Nerve regeneration
Spinal cord injury

ABSTRACT

The current effective method for treatment of spinal cord injury (SCI) is to reconstruct the biological microenvironment by filling the injured cavity area and increasing neuronal differentiation of neural stem cells (NSCs) to repair SCI. However, the method is characterized by several challenges including irregular wounds, and mechanical and electrical mismatch of the material-tissue interface. In the current study, a unique and facile agarose/gelatin/polypyrrole (Aga/Gel/PPy, AGP3) hydrogel with similar conductivity and modulus as the spinal cord was developed by altering the concentration of Aga and PPy. The gelation occurred through non-covalent interactions, and the physically crosslinked features made the AGP3 hydrogels injectable. In vitro cultures showed that AGP3 hydrogel exhibited excellent biocompatibility, and promoted differentiation of NSCs toward neurons whereas it inhibited over-proliferation of astrocytes. The in vivo implanted AGP3 hydrogel completely covered the tissue defects and reduced injured cavity areas. In vivo studies further showed that the AGP3 hydrogel provided a biocompatible microenvironment for promoting endogenous neurogenesis rather than glial fibrosis formation, resulting in significant functional recovery. RNA sequencing analysis further indicated that AGP3 hydrogel significantly modulated expression of neurogenesis-related genes through intracellular Ca^{2+} signaling cascades. Overall, this supramolecular strategy produces AGP3 hydrogel that can be used as favorable biomaterials for SCI repair by filling the cavity and imitating the physiological properties of the spinal cord.

1. Introduction

Spinal cord injury (SCI) may disrupt sensorimotor circuits, thus impairing motor, sensory and autonomic nervous functions [1,2]. As a result, it significantly lowers the quality of life of the affected person and imposes a huge economic and emotional burden to the individuals and families. Approximately half a million people suffer from SCI every year caused by accidents, sports, or falls [3]. SCI is followed by a series of

Peer review under responsibility of KeAi Communications Co., Ltd.
* Corresponding author. Department of Orthopedics Surgery, The Second Affiliated Hospital, School of Medicine, Zhejiang University, Hangzhou, 310009, Zhejiang, China.
** Corresponding author.
*** Corresponding author. Department of Orthopedics Surgery, The Second Affiliated Hospital, School of Medicine, Zhejiang University, Hangzhou, 310009, Zhejiang, China.
E-mail addresses: lifangcai@zju.edu.cn (F. Li), qianzhao@zju.edu.cn (Q. Zhao), zrcqx@zju.edu.cn (Q. Chen).
[1] These authors contributed equally to this work.

https://doi.org/10.1016/j.bioactmat.2021.11.032
Received 10 August 2021; Received in revised form 15 November 2021; Accepted 16 November 2021
Available online 23 December 2021

progressive pathological changes, including edema, hypoxia, ischemia, inflammation, apoptotic and necrotic nerve cell death, culminating in formation of a cytotoxic microenvironment and irregular cystic cavitation, ultimately resulting in further neurological dysfunctions [4,5]. In addition, the harsh microenvironment around the lesion site mainly promotes differentiation of activated endogenous neural stem cells (NSCs) into astrocytes, thus producing glial fibrosis that seals the fluid-filled cystic cavities [6]. As a result, the tissue impairs transmission of electrical signal in living nerve cells in the lesion site [7]. Critically, this damages electric connections across the injured spinal cord, eventually disrupting neural circuits [8]. Therefore, formation of cystic cavities and glial fibrosis significantly limits SCI repair [9].

Injectable hydrogel for treatment of SCI is an effective strategy to promote tissue repair by bridging irregular cystic cavities [9,10]. Furthermore, it mimics the physiological environment of living tissues, thus promoting survival and differentiation of cells [11,12]. However, the spinal cord conducts and transmits bioelectrical signals which facilitate communication with other types of cells through the neural networks and synapse [13]. The neural network participates in differentiation of NSCs and nerve regeneration [14,15]. This prevents scarring of tissues at the injury site and facilitates transmission of biological signals to achieve specific biological functions [16,17]. Therefore, development of injectable and biocompatible hydrogel with similar conductivity and modulus as the spinal cord plays an important role in clinical application for treatment of SCI.

Conductive polymers such as polypyrrole (PPy), polyaniline (PANI) and polythiophene (PEDOT) have previously been developed for nerve tissue engineering. PPy is the most common used polymer in nerve regeneration owing to its high conductivity (up to 10^3 S/cm), and easy synthesis [18]. PPy can be fabricated into different conductive composites through blending with other soft materials [19]. Hydrogels prepared from gelatin (Gel) have several excellent properties which enhance cell adhesion of the whole hydrogel system, and promote proliferation and differentiation of cells [20,21]. Therefore, PPy and Gel can be assembled into biocompatible implant conductive materials. However, it is difficult to maintain its morphology and regulate regenerated nerves due to the dissolution at body temperature, poor mechanical properties, and rapid enzymatic degradation of Gel in vivo [22]. Notably, agarose (Aga) can enhance the mechanical properties and thermal stabilities of hydrogels [23]. In addition, Aga can guide growth of regenerated axons [24]. Physically crosslinked supramolecular hydrogels have attracted considerable attention in tissue engineering fields unlike chemically cross-linked hydrogels. Physicochemical properties of functional supramolecular hydrogels can be effectively modified through noncovalent molecular interactions to achieve the desirable functions owing to their dynamically reversible structure and unique functions [25]. Therefore, with appropriate combination of PPy, Gel and Aga, the obtained hydrogels present similar modulus and conductivity as the spinal cord. Moreover, the hybrid hydrogel can be injectable to fill in arbitrary defects due to the physical crosslinking features [26].

In the current study, an Aga/Gel/PPy (AGP3) hydrogel was developed by altering the concentration of Aga and pyrrole (Py) (Scheme 1A). The hydrogel showed similar conductivity as the spinal cord through the in situ formation of conjugated PPy. Furthermore, addition of Aga promoted the thermal stability of the hydrogel at body temperature which was quite different from the conventional biotoxic chemically crosslinking strategy. The physically crosslinked features made the AGP3 hydrogels injectable, and the modulus was easily adjusted by changing the amount of Aga. In vitro cultures showed that the AGP3 hydrogel exhibited good biocompatibility, and accelerated formation and maturation of neurons whereas it inhibited over-proliferation of astrocytes. Injection of the AGP3 hydrogel in vivo completely covered the tissue defects and reduced injured cavity areas. In vivo studies further showed that the hydrogel provided a biocompatible microenvironment for NSCs migration and differentiation. This characteristic decreased glial fibrosis deposition and activated endogenous NSCs neurogenesis, resulting in significant recovery of motor function (Scheme 1B).

2. Results and discussion

2.1. Fabrication and characterization of hydrogels

The multifunctional conductive hydrogel was prepared using a mixture of $FeCl_3$, Aga, Gel, and Py. The sol-gel transition temperature of final obtained hydrogel was determined based on the mass ratio of Aga and Gel [27]. The Gel concentration was fixed at 5% (w/v) to maintain the shape of hybrid hydrogels at body temperature for subsequent experiments. Further rheological testing showed that the Aga

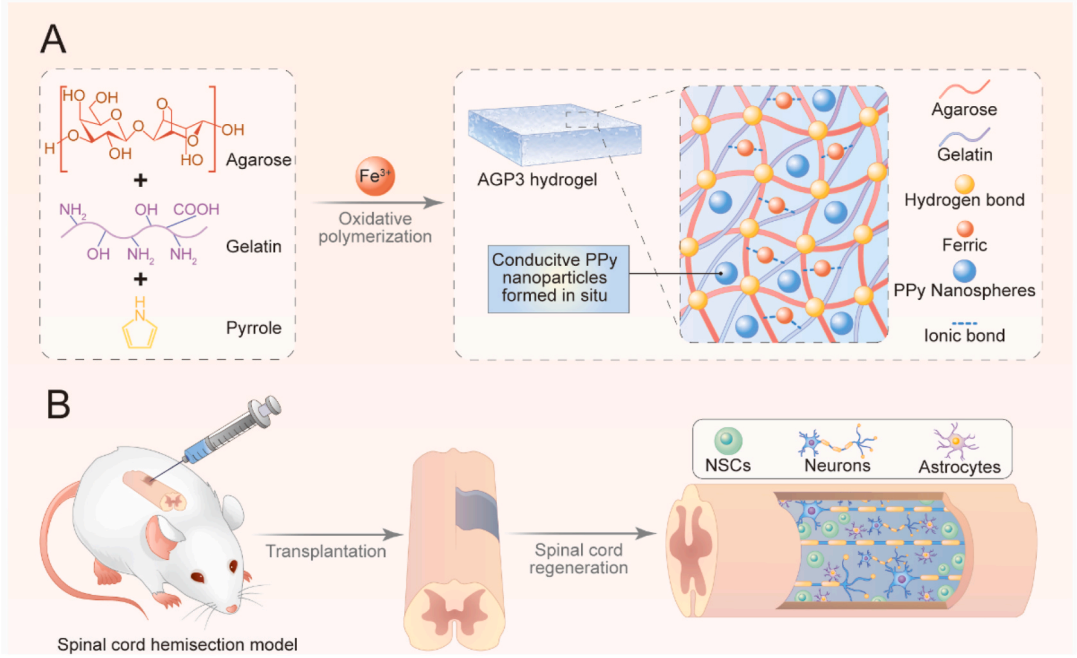

Scheme 1. Schematic illustration of (A) preparation and (B) application of the AGP3 hydrogels to SCI repair.

concentration significantly affected the mechanical properties (Fig. S1A). A 1% (w/v) Aga concentration and the hydrogel showed an average storage modulus (G′) of approximately 560 Pa at 37 °C (Fig. S1B). Therefore, the hydrogel with 1% (w/v) Aga concentration was selected for subsequent experiments. $FeCl_3$ was used as an oxidant for in situ initiation of Py to uniformly obtain conductive PPy and improve conductivity of the hydrogel. For easy description, hydrogels with different Py concentrations were denoted as AG (without Py), AGP1 (low Py content), AGP2 (medium Py content), AGP3 (high Py content). The specific Py concentrations are presented in the experimental section. Furthermore, Fe^{3+} increased the crosslinking densities of hydrogels through ionic interactions with carboxylate and amino groups in Aga and the Gel [28]. Analysis of Energy-dispersive X-ray (EDX) images showed that $FeCl_3$ dispersed in AGP3 hydrogel and was absent in the AG hydrogel (Fig. 1B and Fig. S2). In addition, Fe^{3+} can improve the adhesive properties of the wet hydrogel [29]. The Fourier Transform Infrared (FTIR) spectra (Fig. 1C) of AGP3 hydrogel showed the absorption peak at 1460 and 1550 cm^{-1} which were characteristic peaks of

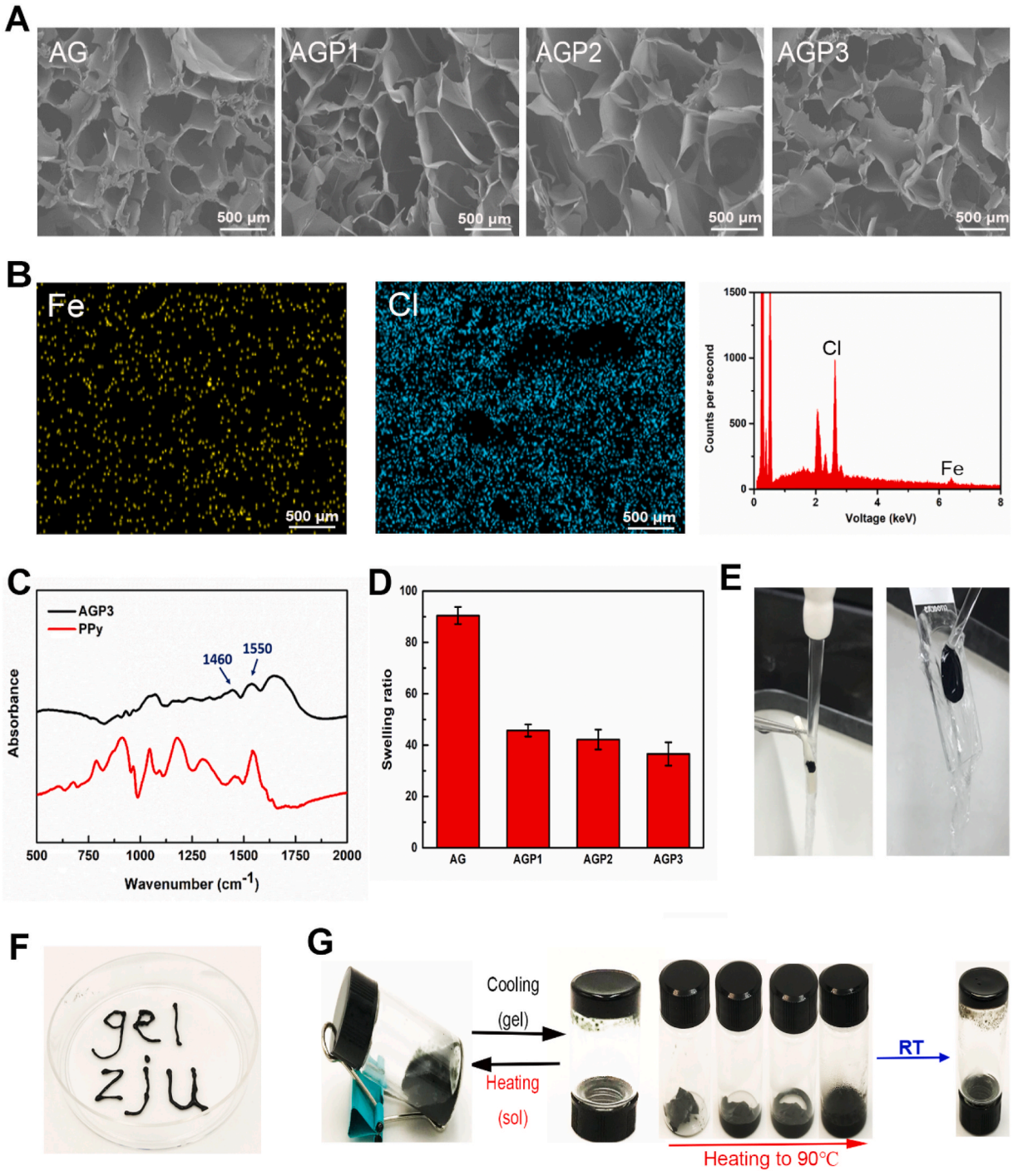

Fig. 1. Characterization of hydrogels. (A) SEM images of AG, AGP1, AGP2 and AGP3 hydrogels. (B) Element analysis of AGP3 hydrogels via EDX. (C) FTIR spectra of PPy powder and AGP3 hydrogel. (D) Swelling ratio of the four types of hydrogels. (E) Photographs showing that the AGP3 hydrogel could adhere tightly to the spinal cord and glass. (F) AGP3 hydrogels were injected by a 26G syringe. (G) Photographic presentation of the thermal reversibilities (sol-gel transition) of the AGP3 hydrogel.

PPy, thus confirming successful synthesis of conductive hydrogel [7,30].

Scanning electron microscopic (SEM) images showed that the hydrogels had interconnected porous structures with various pore sizes (Fig. 1A and Fig. S3). Meanwhile, PPy had no significant effect on the porous structures. These interconnected macro-porous structures could provide adequate space for promoting electron transmission and exchanging of the nutrients and the wastes between the cells and their external environment [31,32]. The swelling behavior of hydrogels is critical to its application in tissue engineering. Swelling intensity of the hydrogel was directly proportional to PPy content (Fig. 1D). Especially, the swelling ratios of the hydrogel ranged from 91.8 for AG to 38.9 for AGP3 with increase in PPy concentration. This difference indicates the hydrophobic feature of the PPy. In addition, further crosslinking by Fe^{3+} would decrease the swelling ratios. Notably, the hydrogels were cross-linked by ionic bonds and hydrogen bonding, implying that they can be easily injected using syringe needles (Fig. 1F and Movie S1). Moreover, the hydrogels adhered tightly to the spinal cord and glass owing to the presence of the Gel (Fig. 1E and Movie S2-3), thereby enhancing the interactions between implanted materials and the surrounding tissue. Furthermore, the hydrogel showed good thermal-reversible properties (Fig. 1G). The hydrogels underwent long-time swelling in PBS at 37 °C, and PPy did not leak from the hydrogel (Fig. S4).

Supplementary video related to this article can be found at https://doi.org/10.1016/j.bioactmat.2021.11.032

The storage modulus (G′) was higher compared with the loss modulus (G″) for all hydrogels throughout the testing frequency range, indicating stable crosslinking networks of the hydrogels (Fig. 2A). The average G′ ranged from 560 Pa for AG hydrogel to 1800 Pa for AGP1 hydrogel. Further increase in Py level slightly reduced the G′, which may be attributed to the decrease in ionic crosslinking points. Regarding electrochemical impedance spectroscopy (EIS), compared with AG, AGP1, and AGP2 hydrogels, AGP3 hydrogels had lower impedance (Fig. 2C). Furthermore, the phase angle of AGP3 hydrogel was lower compared with that of AG hydrogel (Fig. 2D). The conductivity of the AG hydrogel was 0.1×10^{-3} S cm^{-1}, and increased to 0.2×10^{-2} S cm^{-1} after introducing PPy (AGP3) (Fig. 2E). AGP3 hydrogel showed the best electrical conductivity and electron transfer behaviors, attributed to the high PPy contents.

Supramolecular polymer hydrogels are held together by dynamic noncovalent intermolecular forces [33], and can be developed to achieve desirable functions through an elegant combination of different materials [34]. Stiffness of the hydrogel significantly affects the function

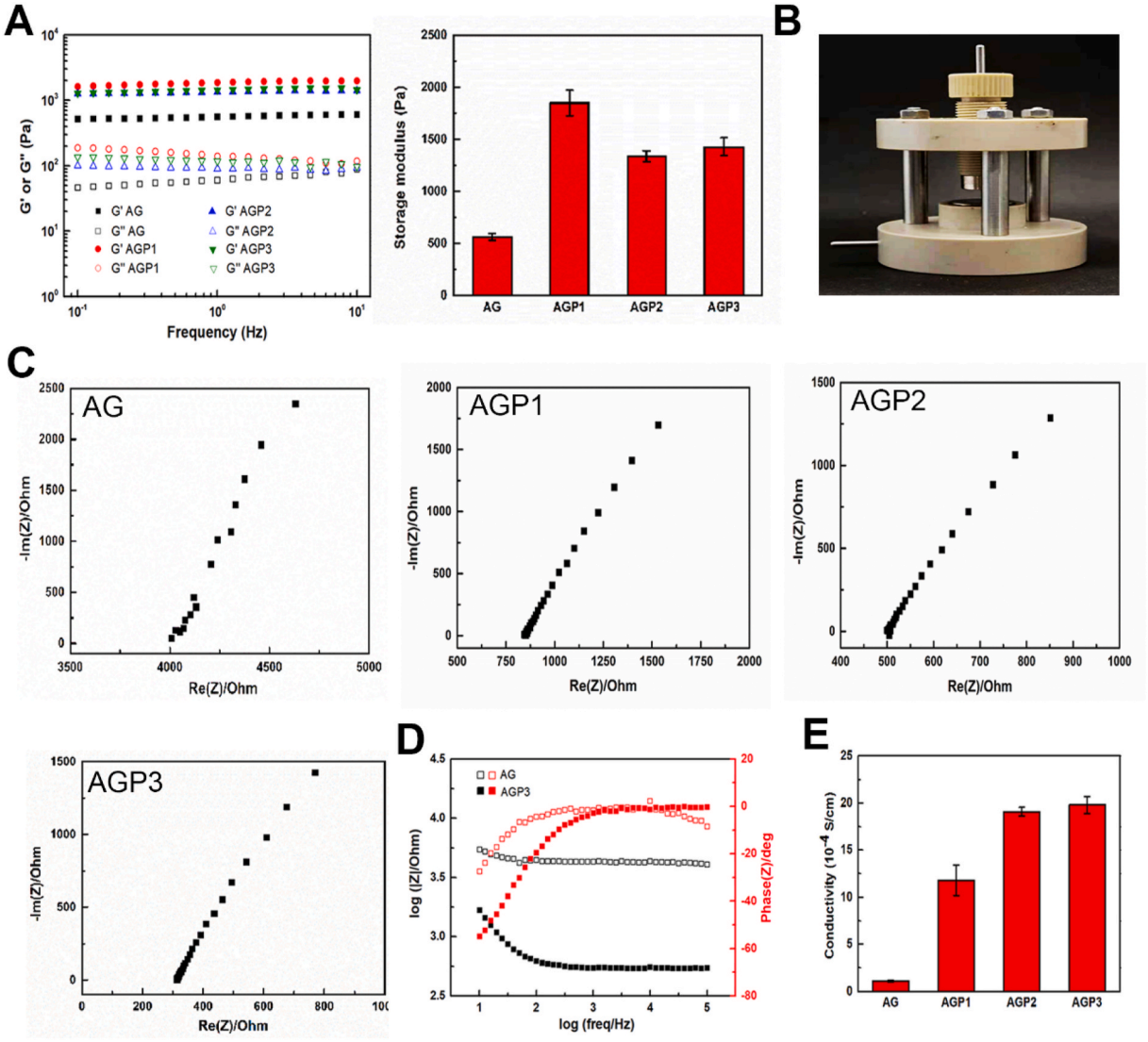

Fig. 2. Electrical and mechanical properties of the hydrogel. (A) The rheological properties of different hydrogels and the related storage modulus. (B) The photo of the custom-made testing mould. (C) The impedances of the four types of hydrogels. (D) Phase curves of the AG and AGP3 hydrogel. (E) The conductivities of hydrogels with different PPy content.

and differentiation of NSCs [32]. NSCs differentiate into neurons in soft hydrogel (≈0.1–1 kPa) whereas they differentiate into astrocytes in hard hydrogel (≈7–10 kPa) [35,36]. On the other hand, a hydrogel with smaller modulus (< 1 kPa) do not hold cell spheroids in place, resulting in the loss of many NSCs from the hydrogel [35]. Further, the modulus of spinal cord tissue is between 100 and 3000 Pa [7,37], which means that hydrogel with ≈1.5 kPa modulus may be an optimal candidate for in vivo applications [35]. In addition, the electrical cue has been corroborated as another significant factor, being able to distinctively aid in inducing the differentiation of NSCs into neurons [38]. Studies report that the conductivity of the normal spinal cord is between 10^{-2} and 10^{-1} S cm^{-1} [7,39]. As aforementioned, AGP3 hydrogels with ideal mechanical strength (1470 Pa) and conductivity (0.2×10^{-2} S cm^{-1}) were developed in the present study by adjusting the amount of Aga and Py. Due to hydrogen bonding, gelation occurred and made the AGP3 hydrogel injectable, which is more suitable for filling irregular geometries created by injury.

2.2. In vitro and in vivo biocompatibility of hydrogels

Fluorescent images of Live/Dead staining showed that approximately 90% of the cells were alive in the four hydrogels (Fig. S7A and B). Findings from CCK-8 assays of the NSCs showed excellent viability in the hydrogels which was consistent with result from Live/Dead staining (Fig. S7E). To verify this finding, EdU assays were used to explore proliferation ability of NSCs. The findings showed colocalization of EdU with Hoechst which indicated newly proliferated cells. Analysis showed no significant difference in proliferation rate of NSCs in the four hydrogels, which was consistent with the staining results (Fig. S7C and D). These findings indicate that the hydrogels were not cytotoxic against NSCs and showed high biocompatibility to NSCs.

Intraneural implants leads to inflammatory response and fibrotic encapsulation. Iba-1 and CD68 are markers for microglia and macrophages, respectively, and are related to acute or chronic neuroinflammation resulting from SCI or exogenous implantation [40,41]. Iba-1^+ and $CD68^+$ cells were detected in all groups at week 2 and week 6 after SCI, indicating presence macrophages/microglia inside and around the injury site. However, we observed that Iba-1 and CD68 expression were qualitatively decreased in AG and AGP3 groups when compared to SCI group (Fig. 3A–D and Fig. S8–9). To explore the rate of deposition of fibroblast scars around the injury site, the level of extracellular matrices such as laminin and fibronectin was determined. The findings showed significant deposition of laminin and fibronectin proteins at the interface between SCI sites and normal areas in the SCI groups (Fig. 3E–H). However, rats in the AG and AGP3 group exhibited significantly less fibrous scar. In general, the AG and AGP3 hydrogel exhibited good biocompatibility in vivo, consistent with in vitro findings. This can be attributed to the mechanical matching of the material-tissue interface, and the cytocompatibility of the hydrogel [42].

2.3. Assessment of glial scar formation in vivo

Reactive astrocytes play a major roles in formation of astroglial scars, which is recognized as an essential factor in hindering SCI repair [43]. The findings showed a high level of $GFAP^+$ cells at the interface between the lesion and normal tissues, at week 2 and 6, which formed glial scar like structures (Fig. 4A–B and Fig. S10). However, the AGP3 group exhibited a significant decrease in the number of GFAP-labeled reactive astrocytes compared with other groups. Additionally, reactive astrocytes secrete inhibitory ECM molecules that induce gliosis, which inhibits migration of NSCs and axon growth [44]. Evaluation of inhibitory chondroitin sulfate proteoglycans (CSPGs) using CS-56 staining showed that CSPGs expression in the AGP3 group was lower than that in AG and SCI groups (Fig. 4C and D).

Astrocytes are activated and mainly transformed to the A1 state by the unfavorable microenvironment after SCI [43]. Active astrocytes secrete nerve regeneration inhibitors such as CSPGs widely distributed in the dense glial scars [45]. The block of glial fibrosis at the injured site disrupts axonal regeneration and growth and normal functioning of the spinal cord after injury [46]. In the present study, high reactive astrogliosis was found at the site of injury in the SCI group, whereas AGP3 hydrogel modulated such phenomenon. In general, AGP3 hydrogels are soft and have almost the same mechanical properties of the spinal cord. AGP3 hydrogels do not promote further damage to the spinal cord tissue, resulting in decreased active astrocytes numbers compared to stiff materials [47]. Moreover, AGP3 hydrogels provide an interface to enable moderate astrocytes attachment, thereby limiting dense activated astrocytes or glial scars into the lesion epicenter [48]. At the same time, AGP3 hydrogels also limit the infiltration of monocytes and macrophages near the lesion edge, thus favorably augmenting the injured microenvironment to reduce astrocytes activation [49,50]. Electroactive biomaterials can also inhibit the astrocytic differentiation of endogenous NSCs, and improve adaptability for the neuronal tissue [51]. As such, the AGP3 hydrogel with soft mechanical and highly conductive properties in the present study can inhibit astrocytes activation in vivo, thereby effectively reducing the CSPGs expression, and resulting in decreased glial scars deposition.

2.4. Assessment of neurogenesis in vitro and in vivo

2.4.1. Immunofluorescence analysis of NSCs and differentiation rate in vitro and in vivo

We employed antibody against β-Tubulin III (Tuj-1) and microtubule-associated protein 2 (MAP-2) to label the newly generated and mature neurons, respectively. As shown in Fig. 5A–C, F, G and Fig. S11, a significantly higher expression level of Tuj-1 and MAP-2 was observed in AGP3 hydrogel group compared with the other three groups. In addition, AGP3 hydrogel induced tight clustering of neurons, which exhibited extensive neurite outgrowth. Further RT-qPCR assay on Tuj-1, MAP-2 and GFAP gene expression levels 7 days after culturing NSCs showed that AGP3 hydrogel increased differentiation of NSCs into neurons, whereas it inhibited astroglial differentiation (Fig. 5D, E and H). The results revealed that AGP3 hydrogel accelerated differentiation of neurons while inhibiting that of astrocytes when compared to other hydrogels.

Distribution of nestin (a marker antibody of NSCs) positive cells in the lesion stie was explored in each group at week 2 and week 6 after injury. The finding showed that abundant endogenous $nestin^+$ cells in the AGP3 group were concentrated at the interface between the lesion and normal tissues (Fig. 6A, D and Fig. S12). In addition, $nestin^+$ cells at the center of the injury site were detected at week 2 and 6 after SCI, indicating that AGP3 hydrogel provided a biocompatible microenvironment for survival and migration of NSCs. Immunofluorescence staining at week 2 and 6 after SCI showed that AGP3 hydrogel increased differentiation of NSCs into neurons (Fig. 6B, E and Fig. S13). Moreover, neural regeneration extended over the entire injured area, creating a continuous neuronal bridge following SCI. Analysis of immunofluorescence staining showed that AGP3 hydrogel upregulated expression of Microtubule-associated protein 2 (MAP-2) and increased maturation of neurons at week 6 after injury (Fig. 6C and F). Further, the number of $MAP\text{-}2^+/NeuN^+$ cells at the lesion site of the rats in the AGP3 group was higher than those in the AG and SCI groups (Fig. S14). In addition, AGP3 group displayed a marked increase in $Tuj\text{-}1^+/EdU^+$ and $NeuN^+/EdU^+$ co-labeled cell density compared with the SCI and AG groups (Fig. 6G–K). Overall, these findings indicate that the endogenous growth-permissive environment reconstituted by the grafted AGP3 hydrogel in the lesion site may promote survival and functional differentiation of endogenous NSCs.

2.4.2. Assessment of axonal regeneration, axonal remyelination, and synapse formation in vivo

Neuronal or axonal regeneration only cannot significantly improve

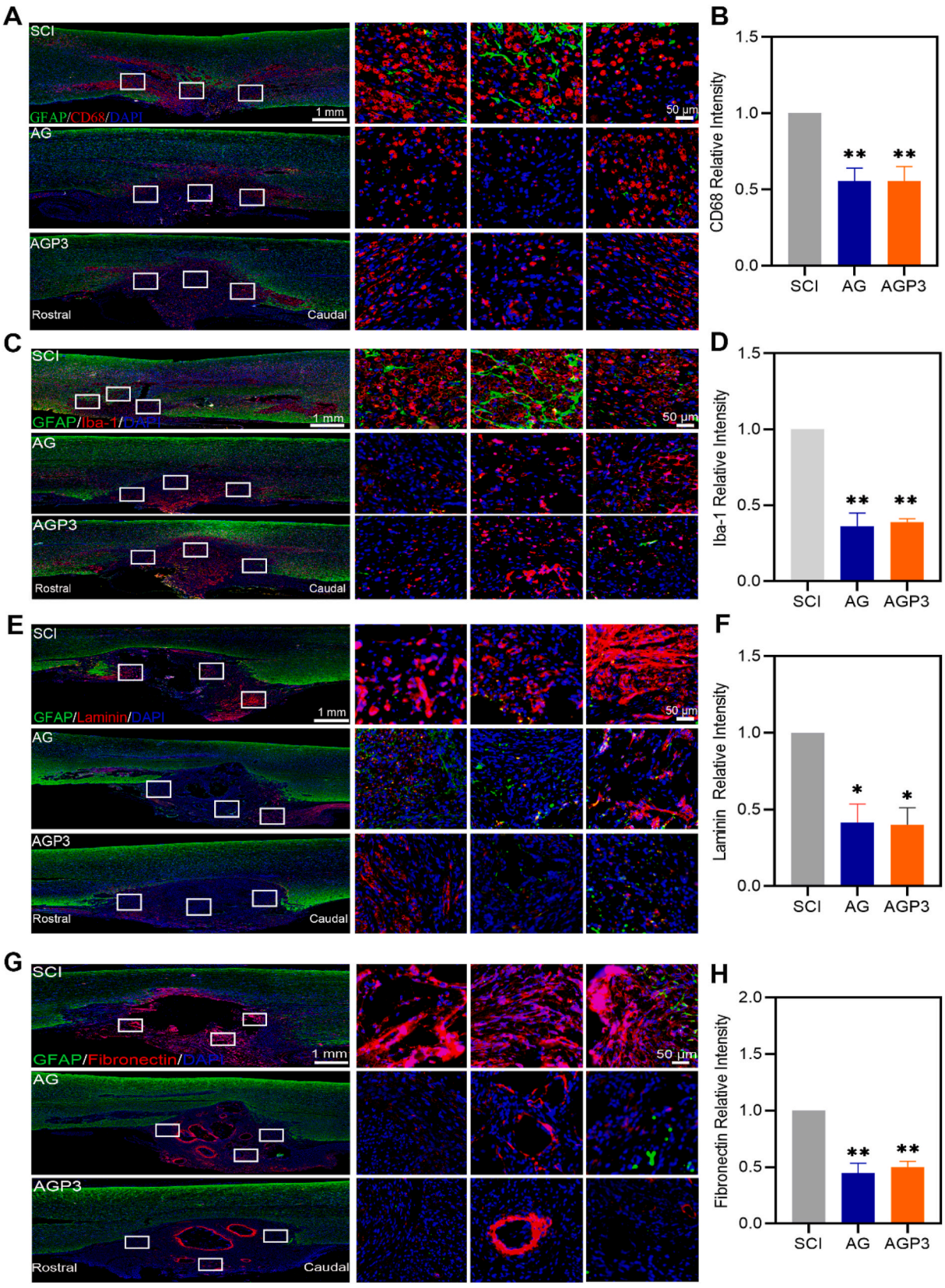

Fig. 3. In vivo biocompatibility assessment. (A) Representative images of tissue sections staining GFAP and CD68 from different groups at 2 weeks after SCI. (B) Quantitative analysis of $CD68^{+}$ cells. (C) Immunofluorescence images of Iba-1/$GFAP^{+}$ cells in different groups at 2 weeks post-surgery. (D) Fluorescence quantitative analysis of Iba-1^{+} cells. (E) Representative images of GFAP and Laminin immunostaining of the spinal cord at 6 weeks after injury. (F) Quantitative data of relative intensities of $Laminin^{+}$ fibroblast scar. (G) Representative images of GFAP and Fibronectin immunostaining of the spinal cord at 6 weeks after injury. (H) Quantitative data of relative intensities of $Fibronectin^{+}$ fibroblast scar at the lesion site.

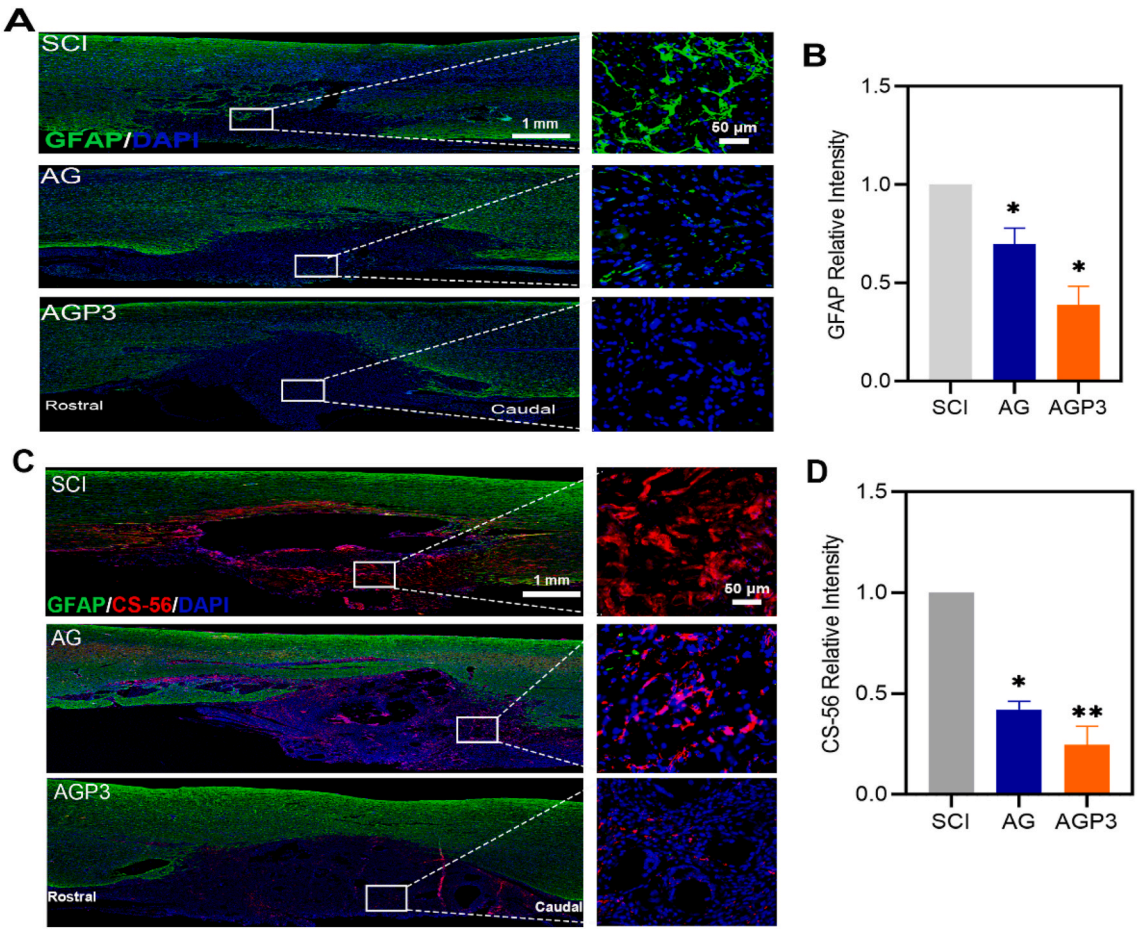

Fig. 4. In vivo glial scar formation assessment. (A) Representative images of tissue sections staining GFAP from different groups at 2 weeks after SCI. (B) Quantitative analysis of GFAP $^{+}$ cells. (C) Images of CS-56 and GFAP immunostaining of spinal sections at 6 weeks after injury. (D) Quantification of relative intensities of CS-56^{+} areas in different groups.

motor function after SCI [52]. It is challenging to fully restore the functioning of the neural circuit of the spinal cord after SCI without re-myelination, synapse formation and expression of neurotransmitters of regenerated axons [53]. We examined the regenerated axonal fibers in the lesion site by staining neurofilament (NF, a marker for nerve fibers) at week 6 post-injury (Fig. S15). Immunofluorescence assay revealed NF-positive fibers were highest in group AGP3, moderate in group AG and lowest in the group SCI. Nerve fibers penetrated the glial cells barrier reaching the core of the injury in the AGP3 group. Growth associated protein-43 (GAP-43) regulates axon elongation, release of neurotransmitters and strengthening of neural plasticity during neural development and regeneration [54]. In the current study, the AGP3 group exhibited the highest GAP-43 expression level compared with the AG and SCI groups (Fig. 7A–C).

Since SCI typically causes destruction of myelin sheath, a microstructure that facilitates rapid signal conduction in axons, remyelination of new axons is a critical process conducive to the recovery of function [40,55]. In addition to nerve regeneration at the implant site, the present study explored remyelination of new axons and synapse formation during neural circuit formation and functional recovery of repaired spinal cord tissue. The findings showed that nerve fibers in the AGP3 group were surrounded by both NF and MBP at higher levels compared with those of AG and SCI groups (Fig. 7D and G). Fig. 7E, H and I showed the ultrathin tissue sections containing the lesion site of spinal cord examined by transmission electron microscopy (TEM). The numbers of small circular structures and the levels of myelin thickness in the AGP3 group were distinctively higher than those in the AG and SCI groups, indicating the formation of newly regenerated axons wrapped in myelin sheaths. Further luxol fast blue (LFB) staining (Fig. 7F and J) showed consistent findings with immunofluorescence staining and TEM results.

In improving neurological function, synaptic connections of the sprouting axons throughout the lesion site may be a vital targeting step [56]. The analysis showed that Syn was overexpressed in the AGP3 group, but was barely detectable in the SCI and AG groups (Fig. 7K and L). Moreover, expression level of NF around nerve fibers was positively correlated with that of Syn. Overall, the present data reveals that synaptic connections and remyelination were present between the newly regenerated axons.

2.4.3. RNA-seq investigations on neurogenesis in vitro

The findings showed that AGP3 hydrogels increased neural differentiation of NSCs, therefore RNA-seq was performed to explore differentially expressed genes (DEGs). A total of 1868 DEGs were identified between cells in AGP3 and control group at day 7 after culture (Fig. S16). A volcano plot showed that out of the 1868 DEGs, 601 genes were upregulated whereas 1267 genes were downregulated. Gene ontology (GO) and heat map analysis showed that some of the overexpressed DEGs such as Bdnf, Neurog2, Wnt7b, Ntrk2, Cobl, Cd200, Htr2a, Nmnat3, Scn1b, Dclk1, Cplx2 and Egr3 in the AGP3 group were implicated in promoting neurogenesis (Fig. 8A and Fig. S17). Kyoto Encyclopedia of Genes and Genomes (KEGG) analysis further showed that the DEGs were implicated in regulation of neuroactive ligand-receptor interaction, Wnt signaling, PI3K-Akt signaling, cAMP signaling, MAPK signaling and calcium signaling pathways (Fig. 8B).

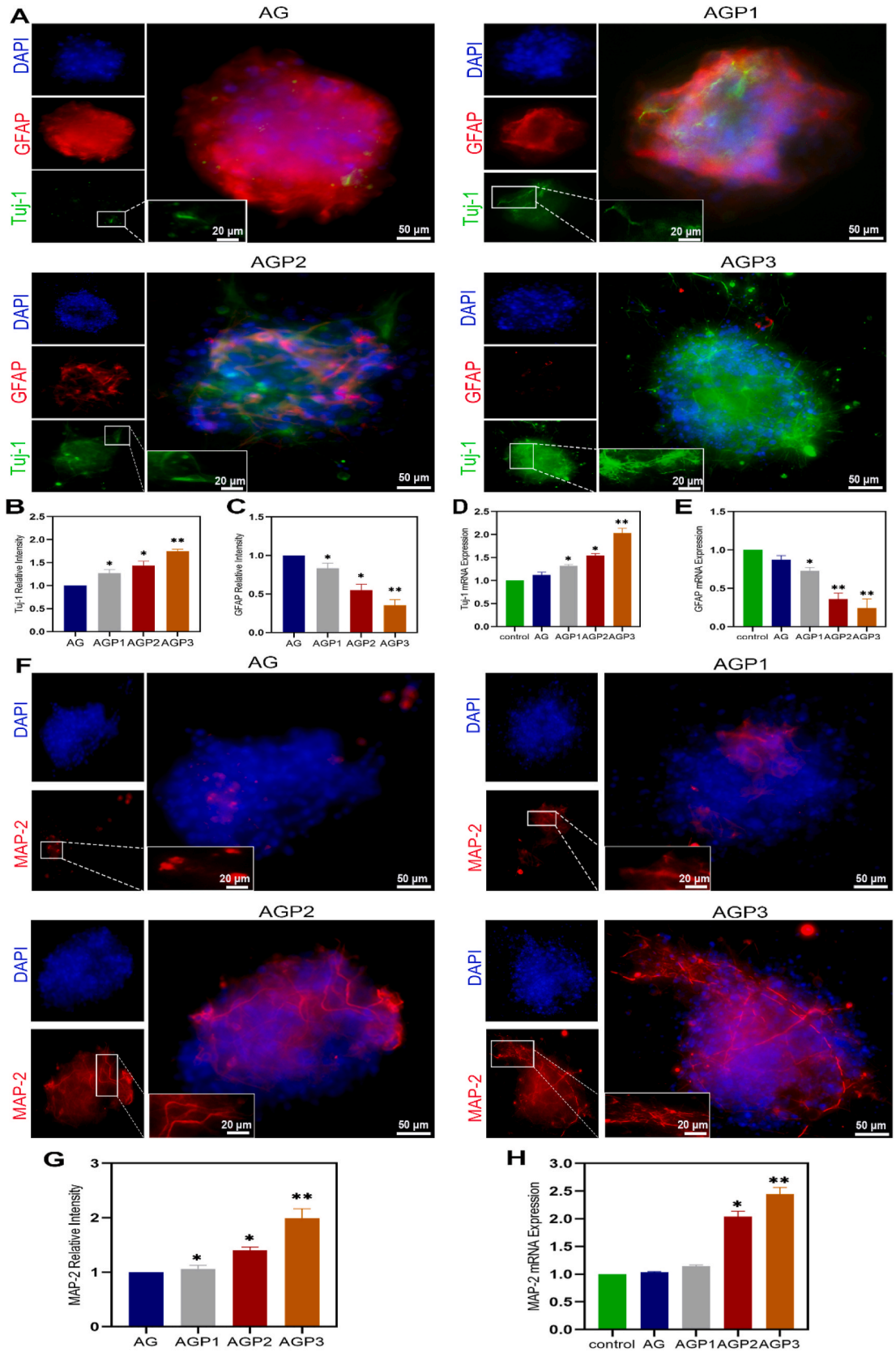

Fig. 5. Immunofluorescence evaluation of NSCs and its differentiation in vitro. (A) Fluorescence images of NSCs differentiation in different hydrogels into Tuj-1$^+$ and GFAP$^+$ cells on day 7. (B, C) Fluorescence quantitative analysis of Tuj-1 and GFAP. (D and E) mRNA expression analysis of Tuj-1 and GFAP. (F) Fluorescence images of NSCs differentiation in different hydrogels into MAP-2$^+$ cells on day 7. (G) Fluorescence quantitative analysis of MAP-2. (H) mRNA expression analysis of MAP-2.

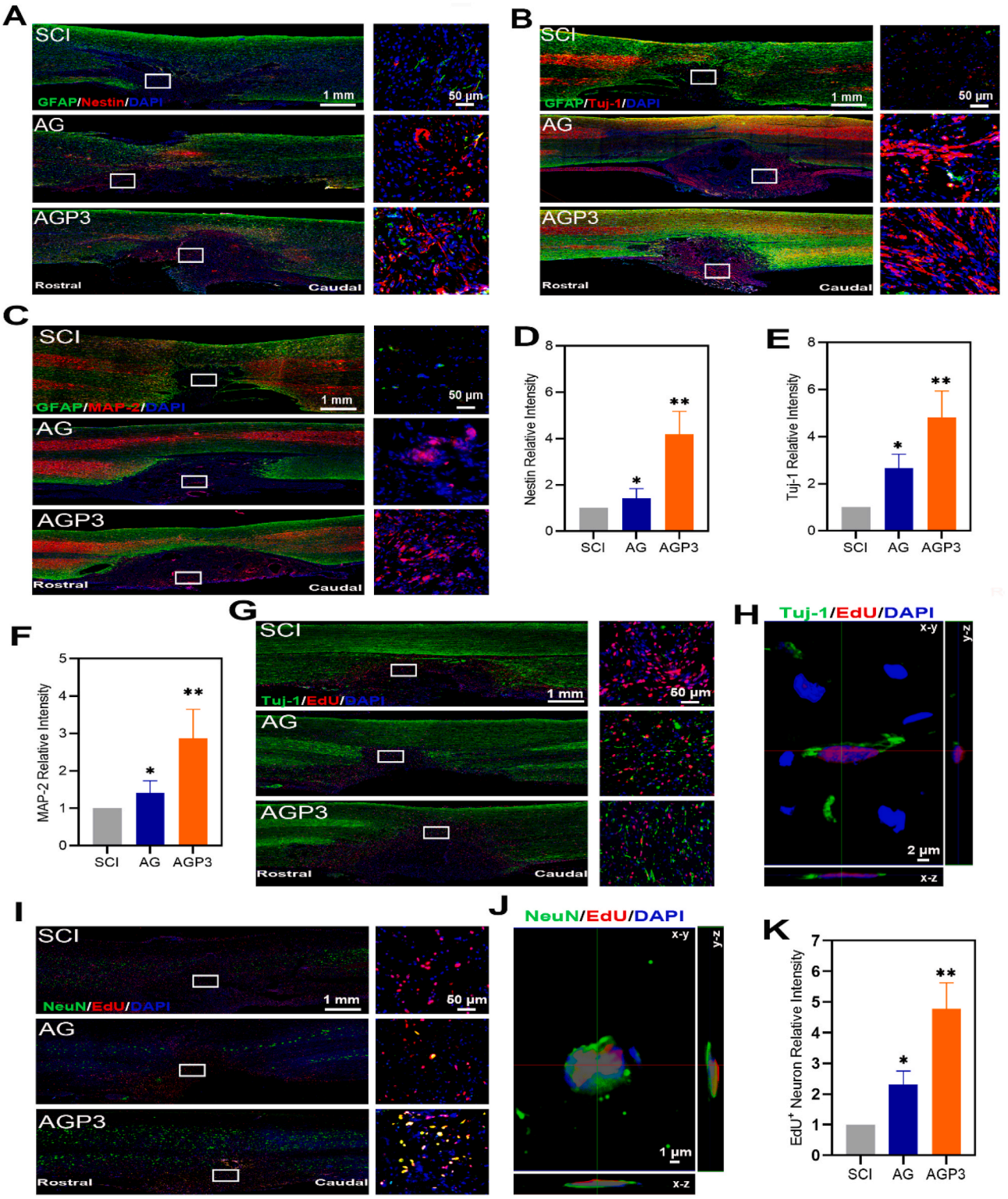

Fig. 6. Immunofluorescence evaluation of NSCs and its differentiation in vivo. (A) Representative images of Nestin and GFAP immunostaining of spinal sections in SCI, AG and AGP3 groups at 2 weeks post-surgery. (B) Representative images of GFAP and Tuj-1 immunostaining of tissue samples at 6 weeks after SCI. (C) Images of GFAP and MAP-2 immunostaining of spinal sections in different groups at 6 weeks after injury. (D) Quantification of relative intensities of Nestin^{+} cells in the lesion site. (E) Quantification of regenerated Tuj-1^{+} neurons in different groups. (F) Quantification of relative intensities of MAP-2^{+} neurons. (G) Representative images of EdU and Tuj-1 immunostaining of tissue samples. (H) Representative confocal Z-stack images showing EdU and Tuj-1 colocalization in the AGP3 group. (I) Representative images of EdU and NeuN immunostaining of spinal sections in different groups. (J) Representative confocal Z-stack images showing EdU and NeuN colocalization in the AGP3 group. (K) Quantification of relative intensities of EdU^{+} neuron.

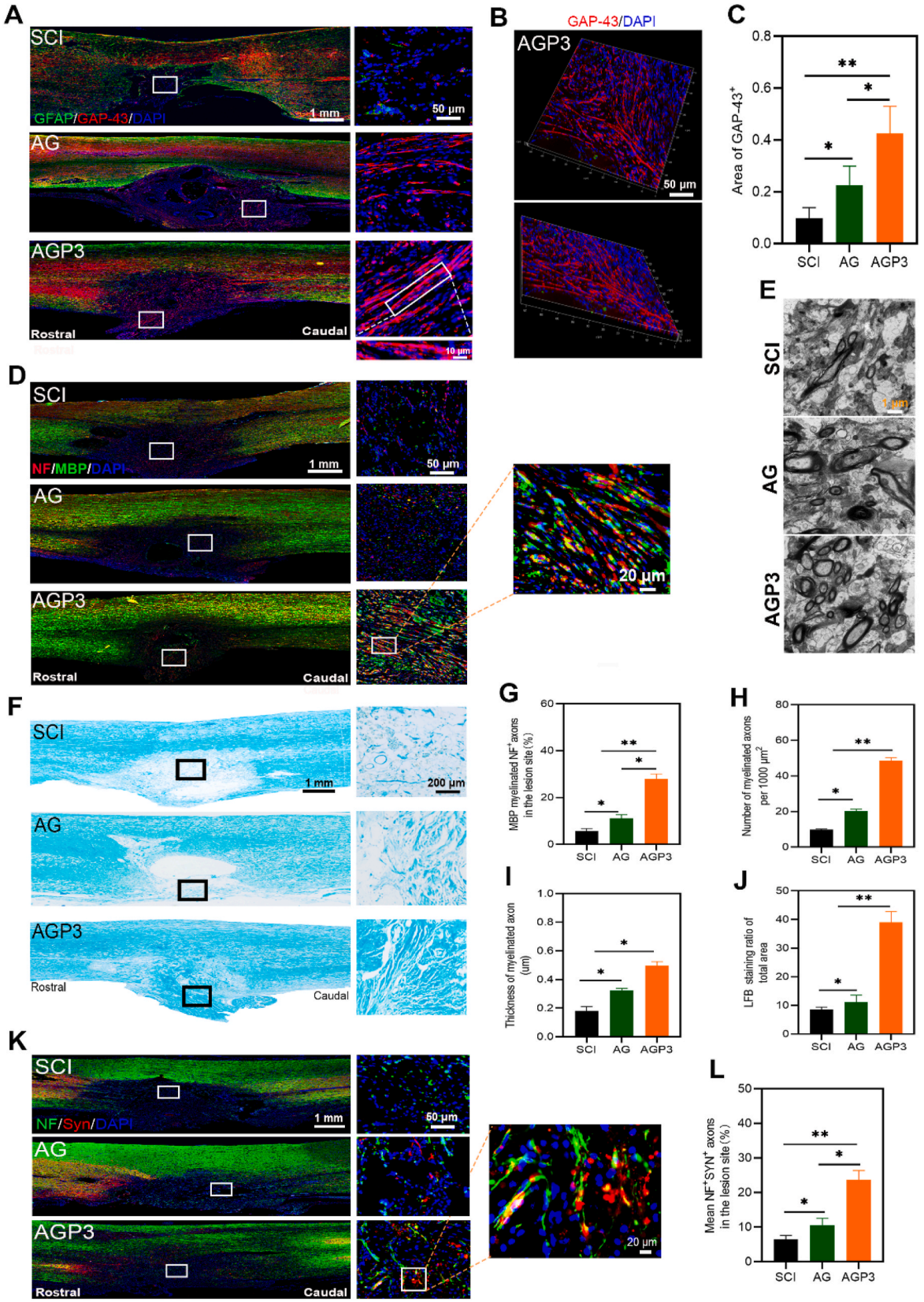

Fig. 7. Assessment of axonal regeneration, axonal remyelination, and synapse formation. (A) Representative images of GAP-43 and GFAP immunostaining of spinal sections in each group at 6 weeks post-surgery. (B) 3D representation of a confocal image of a section in the AGP3 group. (C) Quantification of GAP-43^{+} area at the lesion site. (D) Representative images by double staining with NF/MBP in different groups. (E) Ultrastructural images of the regenerated tissues in the cross sections of the lesion site were assessed by TEM. (F) LFB staining images of spinal sections in each group at 6 weeks postinjury. (G) Quantification of myelinated NF^{+} axons in the lesion site. (H) and (I) show the numbers of the myelinated axons and thickness of the myelin sheets, respectively. (J) Quantification of LFB^{+} area from F in the lesion area. (K) Representative images by double staining with NF/Syn in each group. (L) Quantification of SYN^{+} axons at the SCI sites.

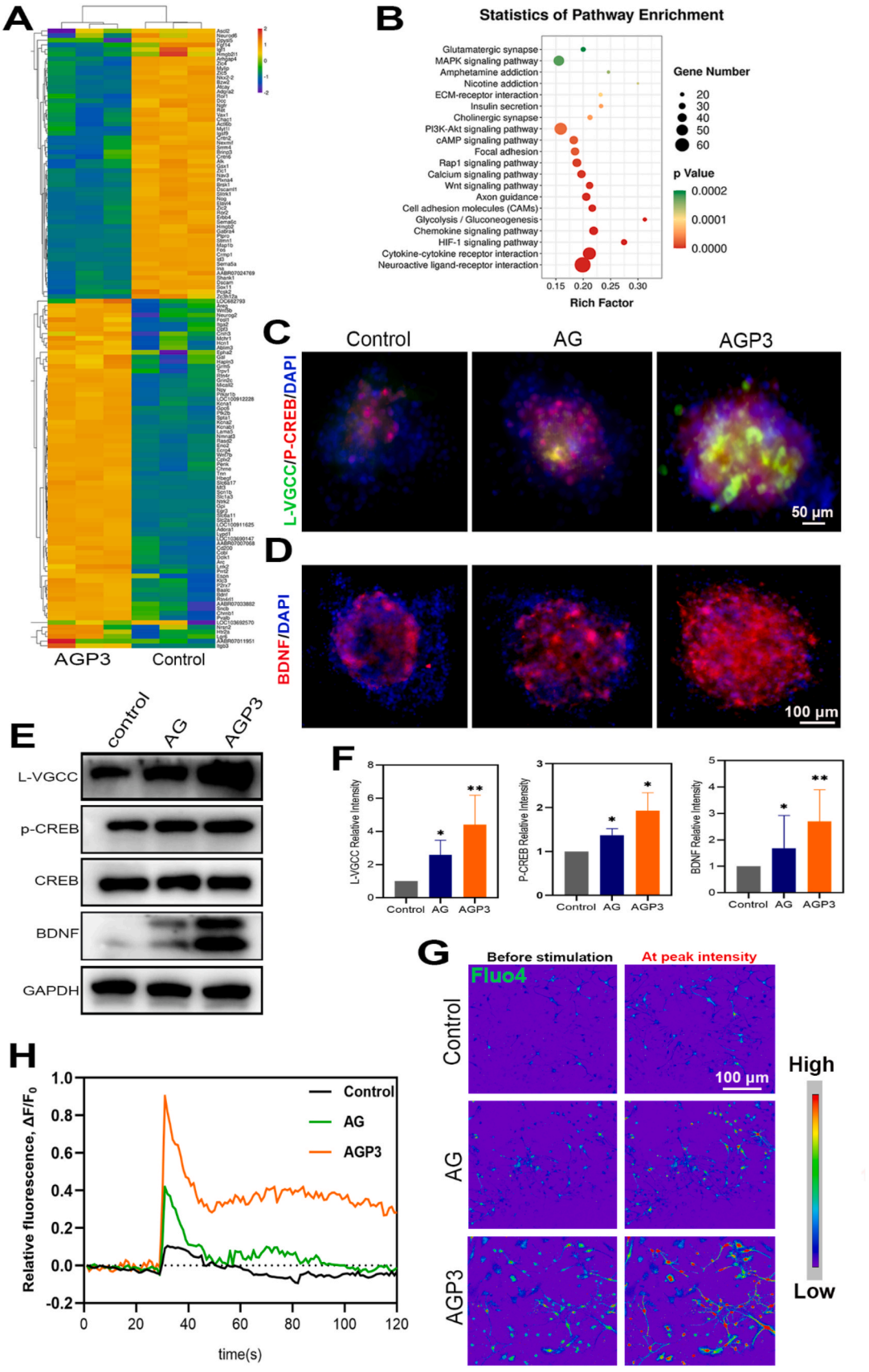

Fig. 8. Investigations of RNA-seq and assessments of intracellular calcium involved in neurogenesis. (A) Heat map of neurogenesis-related gene expression. (B) The gene enrichment KEGG pathway analysis. (C, D) Immunofluorescence images of L-VGCC, *p*-CREB and BDNF in each group on day 7. (E) WB analysis of L-VGCC, *p*-CREB and BDNF. (F) Quantitative analysis of L-VGCC, *p*-CREB and BDNF. (G) Pseudo-color pictures of representative calcium images before and after glutamate stimulation. (H) Image-derived fluo-4 intensity measurements over time in NSCs.

2.4.4. Assessment of intracellular calcium in vitro

To confirm the activation of intracellular Ca^{2+} signaling cascades, gene and protein expression was measured by immunofluorescence staining, RT-qPCR, and WB assay. Analysis showed that AGP3 hydrogel upregulated expression of L-type voltage-gated calcium channel (L-VGCC) implicated in increasing calcium influx in differentiating NSCs (Fig. 8C–H, Fig. S18, and Movie S4-6). Upon exposure to glutamate stimulation, Fluo-4 exhibited the highest fluorescence intensity in group AGP3 compared with the other groups. cAMP-response element-binding protein (CREB) is a transcription factor that regulates several signal transduction and gene expression pathways related to neurogenesis [57]. The findings of the current study showed that AGP3 hydrogel increased expression of *p*-CREB, mediated by the high cellular Ca^{2+} concentration. Moreover, RNA-seq analyses showed that AGP3 hydrogel promoted expression of BDNF and its receptor (Ntrk2) gene. Immunofluorescence staining, WB and qPCR analysis showed that AGP3 hydrogel promoted differentiation of NSCs, which was correlated with high BDNF expression. BDNF protects survival of existing neurons, increases synaptic plasticity, reduces inhibitory properties of proteoglycans in scars, improves growth capability of axons and induces differentiation of new neurons [58,59].

Supplementary video related to this article can be found at https://doi.org/10.1016/j.bioactmat.2021.11.032

To further verify the activation of intracellular Ca^{2+} signaling cascades, NSCs were cultured with a selective L-type calcium channel antagonist (nifedipine). As anticipated, the L-VGCC ion channel was inhibited by Nifedipine, resulting in the decrease of intracellular Ca^{2+} ion influx (Fig. 9A–F and Movie S7-9). In addition, compared with untreated NSCs, the L-VGCC, *p*-CREB and BDNF expression levels of inhibited NSCs decreased. However, the fluorescence intensity of Fluo-4 and the expression levels of L-VGCC, *p*-CREB and BDNF were highest in group AGP3 compared with the other groups, indicating that AGP3 hydrogel could partially reverse the inhibitory effects of Nifedipine. As such, intracellular Ca^{2+} signaling pathway could be assumed to be a significant factor in the effect of AGP3 hydrogel on neurogenesis. (Fig. 9G).

Supplementary video related to this article can be found at https://doi.org/10.1016/j.bioactmat.2021.11.032

After SCI, the formation of scar tissue impedes the migration of endogenous NSCs, which usually differentiate into astrocytes under inhibitory environmental conditions, thereby disrupting neurogenesis [60]. Accordingly, injury-activated endogenous NSCs are considered as a promising candidate for treating SCI by regulating the survival microenvironment and differentiation profiles [61,62]. Biomaterials provide a supportive matrix and biological microenvironment that promote survival and neuronal differentiation of endogenous NSCs, thus establishing nerve connections with the host tissue [63]. The stiffness and electro-activity of the environment are essential determinants of the growth and differentiation of neurons [17,64]. Previous studies report NSCs differentiate into neurons on softer substrates with high conductivity [38]. Consistent findings were observed in the current study in vitro, whereby neurons were more abundant in the AGP3 hydrogel compared with other hydrogels. Therefore, remodeling the endogenous electrical microenvironment of the lesion site can provide new strategies to promote endogenous neurogenesis to construct a neural bridging network [65,66]. Large populations of neurons were generated from endogenous NSCs after transplanting the AGP3 hydrogel into a rat hemisection SCI model, which further rebuild neuronal connectivity. Subsequently, RNA-seq analysis indicated that AGP3 hydrogel significantly strengthened the expression of neurogenesis-related genes, with the potential mechanism being that mechanotransduction mismatches between the material and NSCs significantly alter the cell behavior [67]. Besides stiffness, weak local electric fields produced by cell membranes are enhanced by electroactive material, thereby effectuating transmembrane voltage gradients to influence the ion influx across the cell membrane [65]. Intracellular signaling has a significant influence on the proliferation and differentiation of NSCs [68], which could explain the present findings that neurogenesis was promoted via intracellular Ca^{2+} signaling cascades.

2.5. In vivo functional and histological assessment

Change in structural organizational and pathophysiology affects the functional recovery of the spinal cord. All rats were sacrificed at week 2 and 6 post-surgery. H&E staining (Fig. 10A, C and Fig. S19) and tissue morphology (Fig. 10B) in group SCI displayed severely damaged tissue and significant cystic cavitation compared with rats in groups AG and AGP3. On the contrary, AGP3 hydrogel administration significantly accelerated spinal cord healing, as shown by smaller lesion cavities and better tissue reconnection.

Regenerative effect of AGP3 hydrogel for SCI repair was further explored through functional assessment based on Basso-Beattie-Bresnahan (BBB) scores, footprint test and inclined plane test (IPT) scores. Analysis of BBB scores showed that the right hind limbs of rats in all groups were completely paralyzed after surgery (Fig. 10E) but recovered in varying degrees over time. BBB scores were highest for AGP3 group at all-time points, from week 2 through to week 6 after surgery, indicating that AGP3 hydrogel promoted recovery of motor function. Inclined plane assay was performed to explore locomotor activities of the injured rats. Rats in the AGP3 group could hold longer on steeper planes, compared with rats in SCI and AG groups at week 6 post-surgery (Fig. 10F). Footprint test indicated that AGP3 hydrogel improved recovery and coordination between the forepaw and hind paw (Fig. 10D). Moreover, rats in the AGP3 group coordinated the right hind limb footprint relatively well with less stumbling at week 6 after injury. These findings indicate that AGP3 hydrogel promotes nerve repair, resulting in significant recovery of motor function.

Serotonin (5-HT) axons are motor nerve fibers that descends to the ventral gray matter of the spinal cord. They regulate spinal network activity after SCI, thus accelerating recovery of motor function [8,56]. Further analysis was conducted to explore whether 5-HT axons had extended into the injured site along with GFAP. The results reveal that AG and SCI group exhibited a marked decrease in 5-HT nerve fibers density. In contrast, 5-HT axons could regenerate into the lesion site in the AGP3 group (Fig. 10G and H), thereby partially potentiating recovery of locomotor function after SCI in rats. This could be attributed to the amicable microenvironment produced by AGP3 hydrogel in reducing the reactive astrogliosis and glial scar formation. Moreover, the large pores in the AGP3 hydrogels provide suitable channels for cell migration, which are vital for axonal growth [65,69]. Notably, the present hydrogel did not fully degrade and collapse even after 4 weeks in vivo, which can be considered essential for retaining physical support across the injured site and for supporting and guiding host serotonergic axons through a lesion site [62].

The deficit of motor function after SCI could be attributed to the limited regrowth of the axons in the corticospinal tract (CST) and raphespinal tract (RST) at the region of insult [70,71]. Thus, increasing the sprouting and regrowth of injured or spared CST and RST axons within and beyond the lesion site would likely rebuild functional connections. However, the inhibitory environment constituted by active glial cells producing astroglial scars, myelin debris, and CSPGs prohibits the growth of RST and CST nerve fibers [72]. Therefore, remodeling an endogenous growth-permissive environment of the lesion site can promote sprouting and regrowth of RST and CST axons to restore cortical dependent function. The present AGP3 hydrogels inhibited astrocytes activation in vivo, thereby downregulating repulsive CSPGs, and resulting in decreased glial scars deposition. Such effects could be partially beneficial in reorganizing neural networks lost in the injury, thereby improving the neurological recovery of rats.

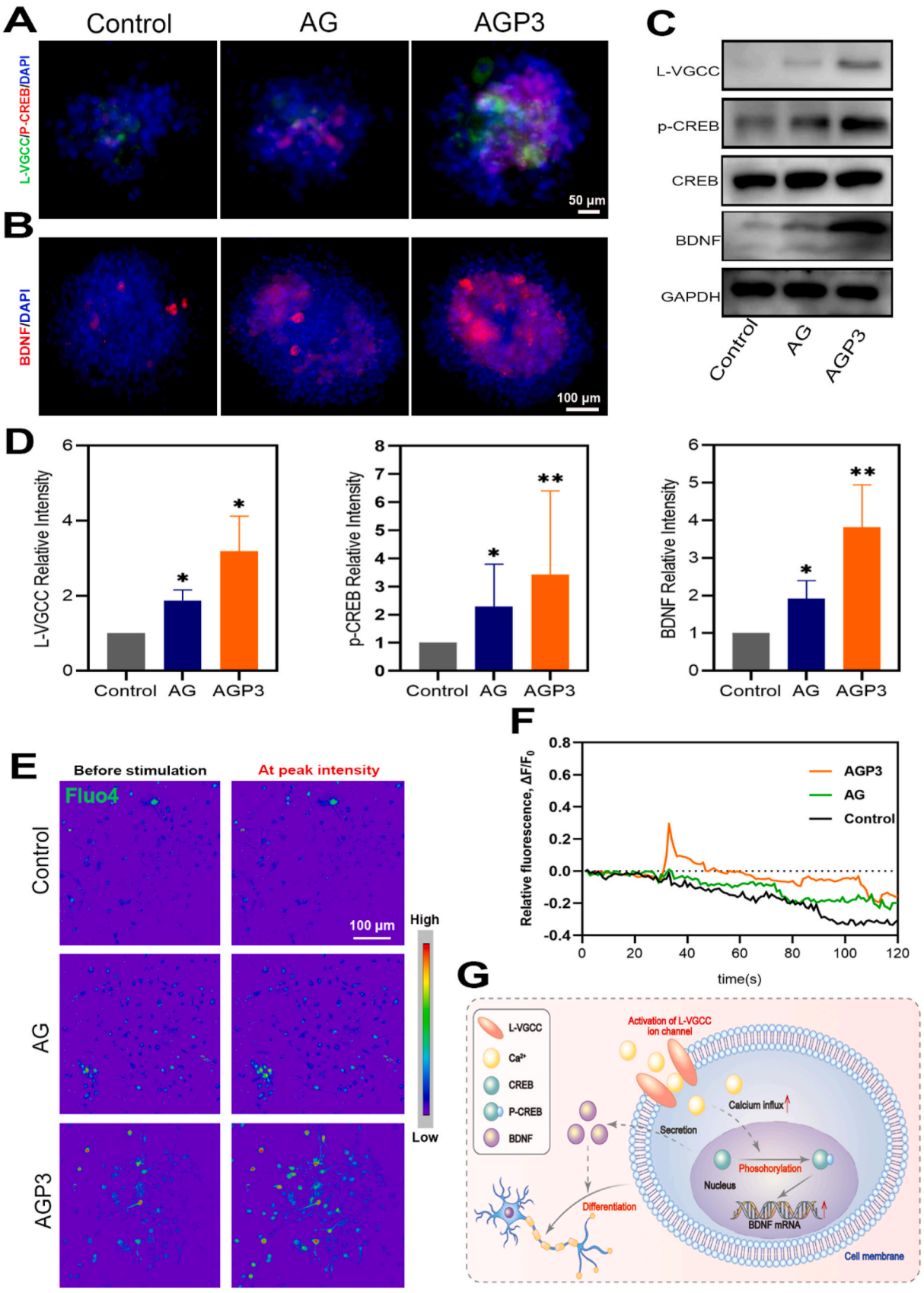

Fig. 9. Assessments of intracellular calcium of NSCs treated with antagonist. (A, B) Immunofluorescence images of L-VGCC, *p*-CREB and BDNF in each group on day 7. (C) WB analysis of L-VGCC, *p*-CREB and BDNF. (D) Quantitative analysis of L-VGCC, *p*-CREB and BDNF. (E) Representative pseudo-color images in nifedipine-treated cells before and after glutamate stimulation. (F) Image-derived fluo-4 intensity measurements over time in nifedipine-treated NSCs. (G) Schematic diagram showing the possible signal transduction pathways of the promoted neurogenesis.

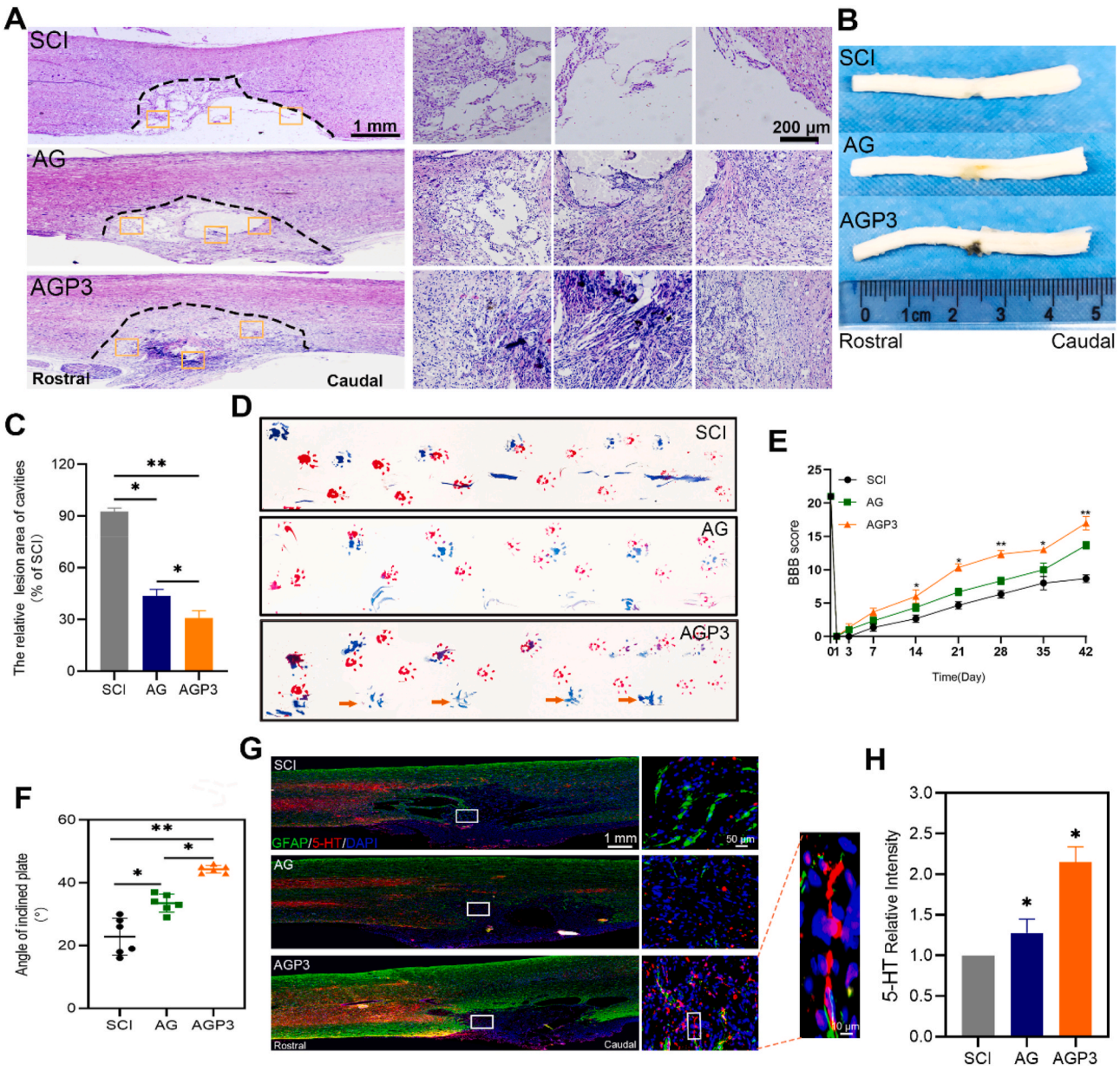

Fig. 10. In vivo functional and histological assessment. (A) Representative images of spinal sections from H&E staining in each group at 6 weeks postinjury. (B) General anatomical analysis of whole spinal cords. (C) Quantification analysis of the lesion site of spinal sections from H&E staining. (D) Photos of forelimb (red) and hindlimb (blue) footprints in each group at 6 weeks postinjury (yellow arrow pointed the posterior limb prints). (E) The BBB scores of the different groups at different time points. (F) The behavior assay of IPT scores at 6 weeks postinjury. (G) Immunofluorescence images by double staining with GFAP/5-HT in each group. (H) Quantification of 5-HT^{+} axons at the SCI sites.

3. Conclusion

In summary, a straightforward and efficient supramolecular strategy was developed to fabricate AGP3 hydrogels satisfying biological and physicochemical requirements by modification of the porosity, modulus, and conductivity. As revealed by in vitro cultures, the AGP3 hydrogels exhibited good biocompatibility, and induced the differentiation of NSCs toward neurons while suppressing the formation of astrocytes. Further, our in vivo results indicate that the injected AGP3 hydrogel could activate the endogenous nerve regeneration of the spinal cord, rather than glial fibrosis formation, to construct a neural bridging network, resulting in significant recovery of motor function. Overall, the supramolecular strategy described in the present study could be used to design biological environment-adaptive functional materials with suitable porosity, modulus, and conductivity, which may be a promising bioactive material for filling the injured cavity area, inhibiting glial scar formation, and promoting neurological function recovery after SCI.

4. Experimental section

4.1. Characterizations

The morphologies of obtained hydrogels were characterized by SEM (SU-3500, HITACHI, Japan) after freezing drying. The chemical structures were identified in the range of 500–4000 cm^{-1} through FTIR (Nicolet 5700, Thermo, USA). Rheological tests were conducted using a rheometer (MARS 60, HAAKE, Germany), at 0.1–10 Hz frequency and 1% strain under 37 °C. The impedance was tested by electrochemical workstation (VMP3, Biologic, France) at the frequency of 10^{1}–10^{5} Hz. During the testing, the counter electrode and reference electrode were

connected together, so that there were two electrodes rather than three. As shown in Fig. 2B, all of the hydrogels were characterized in a custom-made mould (Aida Hengsheng Technology Development Co., Tianjin, China). The corresponding conductivities were converted from resistivities, which were calculated by the x-axis intercepts of the impedance spectrums. Thermogravimetric analysis (Q500, TA, USA) was used to assess the thermal properties of dried hydrogels at a heating rate of 10 °C min^{-1} in air. The swelling of different hydrogels was measured using the conventional gravimetric method. Lyophilized hydrogel of uniform weight, size and shape was immersed into phosphate-buffered saline (PBS) at 37 °C for 24 h to acquire maximum absorption. A filter paper was used to remove excess water, and the new weight of the lyophilized hydrogel was measured. The experiments were performed three times under the same conditions. The swelling ratio of different hydrogels was calculated as follows:

$$\text{Swelling ratio} = \frac{Ws - Wo}{Wo}$$

Where W_S is the swelled weight and W_0 is the dry weight of the hydrogel.

4.2. RNA sequencing (RNA-seq) analyses

NSCs were first cultured for 7 days in differentiation media before extraction of total RNA using Trizol for RNA-seq analysis (LC Bio, Hangzhou, China). To unravel the function of genes regulated by the hydrogel, GO analysis (http://www.geneontology.org) was performed. Bioinformatics analyses were also performed using online OmicStudio tools available at https://www.omicstudio.cn/tool.

4.3. Immunofluorescence staining

After performing antigen retrieval, the longitudinal sections were incubated for 15 min in 0.3% TritonX-100, and blocked for 1 h at 37 °C with 5% BSA in PBS to prevent nonspecific binding of antibodies, which was followed by overnight incubation at 4 °C with specific primary antibodies. After rinsing three times using PBS, the sections were incubated 1 h in the dark at 37 °C with secondary antibody, and then sealed with a Fluoroshield™ Sealant (containing DAPI). A fluorescence microscope (Leica, Wetzlar, Germany) was used to capture the images under the same parameters, and ImageJ software was used to quantify the immunofluorescence intensity. All antibodies used in the present study are listed in Table S1.

4.4. Statistical analysis

The data were expressed as the mean ± standard deviation. ANOVA with Tukey's post hoc test was used for statistical comparisons (Prism 8.0, GraphPad Software). P values less than 0.05 were considered significant (in figures, *$p < 0.05$ and **$p < 0.01$).

CRediT authorship contribution statement

Biao Yang: Conceptualization, Methodology, Formal analysis, Investigation, Writing – original draft. **Chengzhen Liang:** Methodology, Formal analysis. **Di Chen:** Conceptualization, Methodology, Formal analysis, Investigation, Writing – original draft. **Feng Cheng:** Formal analysis. **Yuang Zhang:** Supervision, Writing – review & editing. **Shaoke Wang:** Conceptualization, Supervision. **Jiawei Shu:** Formal analysis. **Xianpeng Huang:** Conceptualization, Supervision. **Jingkai Wang:** Supervision, Writing – review & editing. **Kaishun Xia:** Methodology. **Liwei Ying:** Conceptualization, Supervision. **Kesi Shi:** Formal analysis. **Chenggui Wang:** Conceptualization, Supervision. **Xuhua Wang:** Conceptualization, Supervision. **Fangcai Li:** Conceptualization. **Qian Zhao:** Supervision, Funding acquisition. **Qixin Chen:** Supervision, Funding acquisition.

Declaration of competing interest

The authors declare no conflict of interest.

Acknowledgements

Authors thank Mr. Longxin Li, Dr. Jiapeng Ji and prof. Min Ling for the help of electrochemical testing. Authors also thank the State Key Laboratory of Chemical Engineering for the facilities. Authors thank the Home for Researchers editorial team for polishing our article (www.home-for-researchers.com). This study was financially supported by the Medical and Health Innovation Talent Support Program of Zhejiang Province, China [Grant No. 2020RC011] and the National Natural Science Foundation of China, China [Grant NO. 81772379, 81972096, 81902238, 82002327, 82072465 and 82072481].

Appendix A. Supplementary data

Supplementary data to this article can be found online at https://doi.org/10.1016/j.bioactmat.2021.11.032.

References

[1] P.D. Ganzer, S.C.t. Colachis, M.A. Schwemmer, D.A. Friedenberg, C.F. Dunlap, C. E. Swiftney, A.F. Jacobowitz, D.J. Weber, M.A. Bockbrader, G. Sharma, Restoring the sense of touch using a sensorimotor demultiplexing neural interface, Cell 181 (2020) 763–773 e12.
[2] I. Fischer, J.N. Dulin, M.A. Lane, Transplanting neural progenitor cells to restore connectivity after spinal cord injury, Nat. Rev. Neurosci. 21 (2020) 366–383.
[3] D. Holmes, Spinal-cord injury: spurring regrowth, Nature 552 (2017) S49.
[4] S.L. Lindsay, G.A. McCanney, A.G. Willison, S.C. Barnett, Multi-target approaches to CNS repair: olfactory mucosa-derived cells and heparan sulfates, Nat. Rev. Neurol. 16 (2020) 229–240.
[5] C. Wang, M. Wang, K. Xia, J. Wang, F. Cheng, K. Shi, L. Ying, C. Yu, H. Xu, S. Xiao, C. Liang, F. Li, B. Lei, Q. Chen, A bioactive injectable self-healing anti-inflammatory hydrogel with ultralong extracellular vesicles release synergistically enhances motor functional recovery of spinal cord injury, Bioact. Mater. 6 (2021) 2523–2534.
[6] E. Llorens-Bobadilla, J.M. Chell, P. Le Merre, Y. Wu, M. Zamboni, J. Bergenstrahle, M. Stenudd, E. Sopova, J. Lundeberg, O. Shupliakov, M. Carlen, J. Frisen, A latent lineage potential in resident neural stem cells enables spinal cord repair, Science 370 (2020).
[7] L. Zhou, L. Fan, X. Yi, Z. Zhou, C. Liu, R. Fu, C. Dai, Z. Wang, X. Chen, P. Yu, D. Chen, G. Tan, Q. Wang, C. Ning, Soft conducting polymer hydrogels cross-linked and doped by tannic acid for spinal cord injury repair, ACS Nano 12 (2018) 10957–10967.
[8] L. Yang, B.M. Conley, S.R. Cerqueira, T. Pongkulapa, S. Wang, J.K. Lee, K.B. Lee, Effective modulation of CNS inhibitory microenvironment using bioinspired hybrid-nanoscaffold-based therapeutic interventions, Adv. Mater. 32 (2020), e2002578.
[9] L.T.A. Hong, Y.M. Kim, H.H. Park, D.H. Hwang, Y. Cui, E.M. Lee, S. Yahn, J.K. Lee, S.C. Song, B.G. Kim, An injectable hydrogel enhances tissue repair after spinal cord injury by promoting extracellular matrix remodeling, Nat. Commun. 8 (2017) 533.
[10] G. Courtine, M.V. Sofroniew, Spinal cord repair: advances in biology and technology, Nat. Med. 25 (2019) 898–908.
[11] Y.S. Zhang, A. Khademhosseini, Advances in engineering hydrogels, Science 356 (2017).
[12] J. Chen, D. Wang, L.H. Wang, W. Liu, A. Chiu, K. Shariati, Q. Liu, X. Wang, Z. Zhong, J. Webb, R.E. Schwartz, N. Bouklas, M. Ma, An adhesive hydrogel with "Load-Sharing" effect as tissue bandages for drug and cell delivery, Adv. Mater. 32 (2020), e2001628.
[13] G. Hahn, A. Ponce-Alvarez, G. Deco, A. Aertsen, A. Kumar, Portraits of communication in neuronal networks, Nat. Rev. Neurosci. 20 (2019) 117–127.
[14] M. Bonizzato, G. Pidpruzhnykova, J. DiGiovanna, P. Shkorbatova, N. Pavlova, S. Micera, G. Courtine, Brain-controlled modulation of spinal circuits improves recovery from spinal cord injury, Nat. Commun. 9 (2018) 3015.
[15] C. Wu, A. Liu, S. Chen, X. Zhang, L. Chen, Y. Zhu, Z. Xiao, J. Sun, H. Luo, H. Fan, Cell-laden electroconductive hydrogel simulating nerve matrix to deliver electrical cues and promote neurogenesis, ACS Appl. Mater. Interfaces 11 (2019) 22152–22163.
[16] A. Alves-Sampaio, C. Garcia-Rama, J.E. Collazos-Castro, Biofunctionalized PEDOT-coated microfibers for the treatment of spinal cord injury, Biomaterials 89 (2016) 98–113.
[17] C. Xu, Y. Xu, M. Yang, Y.K. Chang, A.M. Nie, Z.Y. Liu, J.L. Wang, Z.Q. Luo, Black-phosphorus-incorporated hydrogel as a conductive and biodegradable platform for

enhancement of the neural differentiation of mesenchymal stem cells, Adv. Funct. Mater. 30 (2020).
[18] E.A. Kiyotake, M.D. Martin, M.S. Detamore, Regenerative rehabilitation with conductive biomaterials for spinal cord injury, Acta Biomater. (2020). S1742-7061(20)30735-2.
[19] A. Burnstine-Townley, Y. Eshel, N. Amdursky, Conductive scaffolds for cardiac and neuronal tissue engineering: governing factors and mechanisms, Adv. Funct. Mater. 30 (2020).
[20] Y.X. Dong, A. Sigen, M. Rodrigues, X.L. Li, S.H. Kwon, N. Kosaric, S. Khong, Y. S. Gao, W.X. Wang, G.C. Gurtner, Injectable and tunable gelatin hydrogels enhance stem cell retention and improve cutaneous wound healing, Adv. Funct. Mater. 27 (2017).
[21] C. Zhang, M.H. Hsieh, S.Y. Wu, S.H. Li, J. Wu, S.M. Liu, H.J. Wei, R.D. Weisel, H. W. Sung, R.K. Li, A self-doping conductive polymer hydrogel that can restore electrical impulse propagation at myocardial infarct to prevent cardiac arrhythmia and preserve ventricular function, Biomaterials 231 (2020) 119672.
[22] X. Zhao, Y.P. Liang, Y. Huang, J.H. He, Y. Han, B.L. Guo, Physical double-network hydrogel adhesives with rapid shape adaptability, fast self-healing, antioxidant and NIR/pH stimulus-responsiveness for multidrug-resistant bacterial infection and removable wound dressing, Adv. Funct. Mater. 30 (2020).
[23] N. Ninan, A. Forget, V.P. Shastri, N.H. Voelcker, A. Blencowe, Antibacterial and anti-inflammatory pH-responsive tannic acid-carboxylated agarose composite hydrogels for wound healing, ACS Appl. Mater. Interfaces 8 (2016) 28511–28521.
[24] S. Mehrotra, D. Lynam, R. Maloney, K.M. Pawelec, M.H. Tuszynski, I. Lee, C. Chan, J. Sakamoto, Time controlled protein release from layer-by-layer assembled multilayer functionalized agarose hydrogels, Adv. Funct. Mater. 20 (2010) 247–258.
[25] C.S.Y. Tan, J. Liu, A.S. Groombridge, S.J. Barrow, C.A. Dreiss, O.A. Scherman, Controlling spatiotemporal mechanics of supramolecular hydrogel networks with highly branched cucurbit[8]uril polyrotaxanes, Adv. Funct. Mater. 28 (2018).
[26] W.C. Huang, R. Ying, W. Wang, Y.N. Guo, Y.J. He, X.Y. Mo, C.H. Xue, X.Z. Mao, A macroporous hydrogel dressing with enhanced antibacterial and anti-inflammatory capabilities for accelerated wound healing, Adv. Funct. Mater. 30 (2020).
[27] H. Moritaka, K. Nishinari, H. Horiuchi, M. Watase, Rheological properties of aqueous agarose-gelatin gels, J. Texture Stud. 11 (1980) 257–270.
[28] S. Liang, Y. Zhang, H. Wang, Z. Xu, J. Chen, R. Bao, B. Tan, Y. Cui, G. Fan, W. Wang, W. Wang, W. Liu, Paintable and rapidly bondable conductive hydrogels as therapeutic cardiac patches, Adv. Mater. 30 (2018), e1704235.
[29] S. Hong, D. Pirovich, A. Kilcoyne, C.H. Huang, H. Lee, R. Weissleder, Supramolecular metallo-bioadhesive for minimally invasive use, Adv. Mater. 28 (2016) 8675–8680.
[30] C. Wang, S.S. Rubakhin, M.J. Enright, J.V. Sweedler, R.G. Nuzzo, 3D particle-free printing of biocompatible conductive hydrogel platforms for neuron growth and electrophysiological recording, Adv. Funct. Mater. 31 (2021).
[31] Y. Luo, L. Fan, C. Liu, H. Wen, S. Wang, P. Guan, D. Chen, C. Ning, L. Zhou, G. Tan, An injectable, self-healing, electroconductive extracellular matrix-based hydrogel for enhancing tissue repair after traumatic spinal cord injury, Bioact. Mater. 7 (2022) 98–111.
[32] Y.F. Ma, M. Lin, G.Y. Huang, Y.H. Li, S.Q. Wang, G.Q. Bai, T.J. Lu, F. Xu, 3D spatiotemporal mechanical microenvironment: a hydrogel-based platform for guiding stem cell fate, Adv. Mater. 30 (2018).
[33] R.J. Dong, Y.F. Zhou, X.H. Huang, X.Y. Zhu, Y.F. Lu, J. Shen, Functional supramolecular polymers for biomedical applications, Adv. Mater. 27 (2015) 498–526.
[34] X. Dou, N. Mehwish, C. Zhao, J. Liu, C. Xing, C. Feng, Supramolecular hydrogels with tunable chirality for promising biomedical applications, Acc. Chem. Res. 53 (2020) 852–862.
[35] T.C. Tseng, L. Tao, F.Y. Hsieh, Y. Wei, I.M. Chiu, S.H. Hsu, An injectable, self-healing hydrogel to repair the central nervous system, Adv. Mater. 27 (2015) 3518–3524.
[36] L. Fan, C. Liu, X. Chen, Y. Zou, Z. Zhou, C. Lin, G. Tan, L. Zhou, C. Ning, Q. Wang, Directing induced pluripotent stem cell derived neural stem cell fate with a three-dimensional biomimetic hydrogel for spinal cord injury repair, ACS Appl. Mater. Interfaces 10 (2018) 17742–17755.
[37] A. Banerjee, M. Arha, S. Choudhary, R.S. Ashton, S.R. Bhatia, D.V. Schaffer, R. S. Kane, The influence of hydrogel modulus on the proliferation and differentiation of encapsulated neural stem cells, Biomaterials 30 (2009) 4695–4699.
[38] C. Xu, Y.K. Chang, P. Wu, K. Liu, X.Z. Dong, A.M. Nie, C.P. Mu, Z.Y. Liu, H.L. Dai, Z. Q. Luo, Two-dimensional-germanium phosphide-reinforced conductive and biodegradable hydrogel scaffolds enhance spinal cord injury repair, Adv. Funct. Mater. 31 (41) (2021), 2104440.
[39] J. Holsheimer, Computer modelling of spinal cord stimulation and its contribution to therapeutic efficacy, Spinal Cord 36 (1998) 531–540.
[40] J. Luo, X. Shi, L. Li, Z. Tan, F. Feng, J. Li, M. Pang, X. Wang, L. He, An injectable and self-healing hydrogel with controlled release of curcumin to repair spinal cord injury, Bioact. Mater. 6 (2021) 4816–4829.
[41] C. Wang, H. Yue, Q. Feng, B. Xu, L. Bian, P. Shi, Injectable nanoreinforced shape-memory hydrogel system for regenerating spinal cord tissue from traumatic injury, ACS Appl. Mater. Interfaces 10 (2018) 29299–29307.
[42] A.E. Rochford, A. Carnicer-Lombarte, V.F. Curio, G.G. Williams, D.G. Barone, When bio meets technology: biohybrid neural interfaces, Adv. Mater. 32 (2020).
[43] M.B. Orr, J.C. Gensel, Spinal cord injury scarring and inflammation: therapies targeting glial and inflammatory responses, Neurotherapeutics 15 (2018) 541–553.
[44] C.M. Chen, J.C. Tang, Y. Gu, L.L. Liu, X.Z. Liu, L.F. Deng, C. Martins, B. Sarmento, W.G. Cui, L. Chen, Bioinspired hydrogel electrospun fibers for spinal cord regeneration, Adv. Funct. Mater. 29 (2019).
[45] K. Xi, Y. Gu, J.C. Tang, H. Chen, Y. Xu, L. Wu, F. Cai, L.F. Deng, H.L. Yang, Q. Shi, W.G. Cui, L. Chen, Microenvironment-responsive immunoregulatory electrospun fibers for promoting nerve function recovery, Nat. Commun. 11 (2020).
[46] M. Hara, K. Kobayakawa, Y. Ohkawa, H. Kumamaru, K. Yokota, T. Saito, K. Kijima, S. Yoshizaki, K. Harimaya, Y. Nakashima, S. Okada, Interaction of reactive astrocytes with type I collagen induces astrocytic scar formation through the integrin-N-cadherin pathway after spinal cord injury, Nat. Med. 23 (2017) 818–828.
[47] I.R. Minev, P. Musienko, A. Hirsch, Q. Barraud, N. Wenger, E.M. Moraud, J. Gandar, M. Capogrosso, T. Milekovic, L. Asboth, R.F. Torres, N. Vachicouras, Q. Liu, N. Pavlova, S. Duis, A. Larmagnac, J. Voros, S. Micera, Z. Suo, G. Courtine, S.P. Lacour, Biomaterials. Electronic dura mater for long-term multimodal neural interfaces, Science 347 (2015) 159–163.
[48] L. Maiolo, V. Guarino, E. Saracino, A. Convertino, M. Melucci, M. Muccini, L. Ambrosio, R. Zamboni, V. Benfenati, Glial interfaces: advanced materials and devices to uncover the role of astroglial cells in brain function and dysfunction, Adv. Healthc. Mater. 10 (2021), e2001268.
[49] T.M. O'Shea, A.L. Wollenberg, J.H. Kim, Y. Ao, T.J. Deming, M.V. Sofroniew, Foreign body responses in mouse central nervous system mimic natural wound responses and alter biomaterial functions, Nat. Commun. 11 (2020) 6203.
[50] E. Song, J. Li, S.M. Won, W. Bai, J.A. Rogers, Materials for flexible bioelectronic systems as chronic neural interfaces, Nat. Mater. 19 (2020) 590–603.
[51] N. Alegret, A. Dominguez-Alfaro, J.M. Gonzalez-Dominguez, B. Arnaiz, U. Cossio, S. Bosi, E. Vazquez, P. Ramos-Cabrer, D. Mecerreyes, M. Prato, Three-dimensional conductive scaffolds as neural prostheses based on carbon nanotubes and polypyrrole, Acs Appl. Mater. Inter. 10 (2018) 43904–43914.
[52] G. Li, B. Zhang, J.H. Sun, L.Y. Shi, M.Y. Huang, L.J. Huang, Z.J. Lin, Q.Y. Lin, B. Q. Lai, Y.H. Ma, B. Jiang, Y. Ding, H.B. Zhang, M.X. Li, P. Zhu, Y.Q. Wang, X. Zeng, Y.S. Zeng, An NT-3-releasing bioscaffold supports the formation of TrkC-modified neural stem cell-derived neural network tissue with efficacy in repairing spinal cord injury, Bioact. Mater. 6 (2021) 3766–3781.
[53] P. Lu, Y. Wang, L. Graham, K. McHale, M. Gao, D. Wu, J. Brock, A. Blesch, E. S. Rosenzweig, L.A. Havton, B. Zheng, J.M. Conner, M. Marsala, M.H. Tuszynski, Long-distance growth and connectivity of neural stem cells after severe spinal cord injury, Cell 150 (2012) 1264–1273.
[54] K. Xi, Y. Gu, J. Tang, H. Chen, Y. Xu, L. Wu, F. Cai, L. Deng, H. Yang, Q. Shi, W. Cui, L. Chen, Microenvironment-responsive immunoregulatory electrospun fibers for promoting nerve function recovery, Nat. Commun. 11 (2020) 4504.
[55] T.Y. Yuan, Y. Shao, X. Zhou, Q. Liu, Z.C. Zhu, B.N. Zhou, Y.C. Dong, N. Stephanopoulos, S.B. Gui, H. Yan, D.S. Liu, Highly permeable DNA supramolecular hydrogel promotes neurogenesis and functional recovery after completely transected spinal cord injury, Adv. Mater. 33 (2021).
[56] D. Liu, X. Li, Z. Xiao, W. Yin, Y. Zhao, J. Tan, B. Chen, X. Jiang, J. Dai, Different functional bio-scaffolds share similar neurological mechanism to promote locomotor recovery of canines with complete spinal cord injury, Biomaterials 214 (2019) 119230.
[57] H. Wang, J. Xu, P. Lazarovici, R. Quirion, W. Zheng, cAMP response element-binding protein (CREB): a possible signaling molecule link in the pathophysiology of Schizophrenia, Front. Mol. Neurosci. 11 (2018) 255.
[58] F. Huang, T. Chen, J. Chang, C. Zhang, F. Liao, L. Wu, W. Wang, Z. Yin, A conductive dual-network hydrogel composed of oxidized dextran and hyaluronic-hydrazide as BDNF delivery systems for potential spinal cord injury repair, Int. J. Biol. Macromol. 167 (2021) 434–445.
[59] Z. He, H. Zang, L. Zhu, K. Huang, T. Yi, S. Zhang, S. Cheng, An anti-inflammatory peptide and brain-derived neurotrophic factor-modified hyaluronan-methylcellulose hydrogel promotes nerve regeneration in rats with spinal cord injury, Int. J. Nanomed. 14 (2019) 721–732.
[60] Y. Yang, Y. Fan, H. Zhang, Q. Zhang, Y. Zhao, Z. Xiao, W. Liu, B. Chen, L. Gao, Z. Sun, X. Xue, M. Shu, J. Dai, Small molecules combined with collagen hydrogel direct neurogenesis and migration of neural stem cells after spinal cord injury, Biomaterials 269 (2021) 120479.
[61] W. Liu, B. Xu, W. Xue, B. Yang, Y. Fan, B. Chen, Z. Xiao, X. Xue, Z. Sun, M. Shu, Q. Zhang, Y. Shi, Y. Zhao, J. Dai, A functional scaffold to promote the migration and neuronal differentiation of neural stem/progenitor cells for spinal cord injury repair, Biomaterials 243 (2020) 119941.
[62] J. Koffler, W. Zhu, X. Qu, O. Platoshyn, J.N. Dulin, J. Brock, L. Graham, P. Lu, J. Sakamoto, M. Marsala, S. Chen, M.H. Tuszynski, Biomimetic 3D-printed scaffolds for spinal cord injury repair, Nat. Med. 25 (2019) 263–269.
[63] T. Fuhrmann, P.N. Anandakumaran, M.S. Shoichet, Combinatorial therapies after spinal cord injury: how can biomaterials help? Adv. Healthc. Mater. 6 (2017).
[64] A. Higuchi, S.S. Kumar, G. Benelli, Q.D. Ling, H.F. Li, A.A. Alarfaj, M. A. Munusamy, T.C. Sung, Y. Chang, K. Murugan, Biomaterials used in stem cell therapy for spinal cord injury, Prog. Mater. Sci. 103 (2019) 374–424.
[65] W. Xue, W. Shi, Y. Kong, M. Kuss, B. Duan, Anisotropic scaffolds for peripheral nerve and spinal cord regeneration, Bioact. Mater. 6 (2021) 4141–4160.
[66] J. Wang, X. Kong, Q. Li, C. Li, H. Yu, G. Ning, Z. Xiang, Y. Liu, S. Feng, The Spatial Arrangement of Cells in a 3D-Printed Biomimetic Spinal Cord Promotes Directional Differentiation and Repairs the Motor Function after Spinal Cord Injury, Biofabrication, 2021.
[67] W. Ong, N. Marinval, J. Lin, M.H. Nai, Y.S. Chong, C. Pinese, S. Sajikumar, C. T. Lim, C. Ffrench-Constant, M.E. Bechler, S.Y. Chew, Biomimicking fiber platform with tunable stiffness to study mechanotransduction reveals stiffness enhances

oligodendrocyte differentiation but impedes myelination through YAP-dependent regulation, Small 16 (2020), e2003656.
[68] R. Guo, S. Zhang, M. Xiao, F. Qian, Z. He, D. Li, X. Zhang, H. Li, X. Yang, M. Wang, R. Chai, M. Tang, Accelerating bioelectric functional development of neural stem cells by graphene coupling: implications for neural interfacing with conductive materials, Biomaterials 106 (2016) 193–204.
[69] L. Huang, Y. Wang, M. Zhu, X. Wan, H. Zhang, T. Lei, A. Blesch, S. Liu, Anisotropic alginate hydrogels promote axonal growth across chronic spinal cord transections after scar removal, ACS Biomater. Sci. Eng. 6 (2020) 2274–2286.
[70] G.H.D. Poplawski, R. Kawaguchi, E. Van Niekerk, P. Lu, N. Mehta, P. Canete, R. Lie, I. Dragatsis, J.M. Meves, B. Zheng, G. Coppola, M.H. Tuszynski, Injured adult neurons regress to an embryonic transcriptional growth state, Nature 581 (2020) 77–82.
[71] Q. Han, Y. Xie, J.D. Ordaz, A.J. Huh, N. Huang, W. Wu, N. Liu, K.A. Chamberlain, Z.H. Sheng, X.M. Xu, Restoring cellular energetics promotes axonal regeneration and functional recovery after spinal cord injury, Cell Metabol. 31 (2020) 623–641 e8.
[72] F. Li, A. Sami, H.N. Noristani, K. Slattery, J. Qiu, T. Groves, S. Wang, K. Veerasammy, Y.X. Chen, J. Morales, P. Haynes, A. Sehgal, Y. He, S. Li, Y. Song, Glial metabolic rewiring promotes axon regeneration and functional recovery in the central nervous system, Cell Metabol. 32 (2020) 767–785 e7.